scientific reports

OPEN

Non-contact measurement method of liquid composition using microwave radar cross-section

Weijia Zhang[1,2,3,8], Xuejing Cao[1,8], Xue Cheng[1], Tianfang Wei[1,4], Dongqin Sun[1], Zhaowei Wang[2,5], Nutapong Somjit[2,6], Calvin Choi[7] & Shaomin Cai[5]✉

This study aims to provide a non-contact detection of liquid composition inside containers using Microwave Radar Cross-section (RCS) measurement technology. Firstly, it analyzes the limitations of traditional near-infrared spectroscopy methods and proposes the necessity of introducing microwave detection methods. The research demonstrates through experiments a significant correlation between polar substances like total acid content and radar scattering capability, showing microwave radar's effectiveness in reflecting the polarity characteristics of liquids. Furthermore, theoretical derivations and experimental validations illustrate that differences in electromagnetic properties of different liquid components lead to variations in echo loss, thereby impacting RCS levels. Experimental results indicate that microwave radar RCS measurement technology achieves an accuracy level of 2%, capable of distinguishing between different concentrations of ethanol, acetic acid, and other solutions. This study highlights the significant advantages of microwave radar RCS measurement technology in non-contact detection of liquid composition, providing new methods and a technological foundation for precise liquid component detection.

Keywords Microwave Radar Cross-section, Liquid polarity, Correlation analysis

Background and significance

In fields such as chemical engineering, food processing, and pharmaceuticals, many liquids exhibit a high susceptibility to spoilage during processing or storage[1]. Therefore, it is crucial to perform non-contact measurements of the liquid components inside containers. For instance, in the production of beverages like alcohol or milk, strictly controlling the content of each component is essential because variations can affect subsequent processing steps and directly impact product quality. When developing new products or adjusting formulations, precise control of component concentrations is necessary to evaluate the effects of different formulations on the product, ensuring that the quality and flavor meet the required standards.

Traditional methods for detecting liquid components, such as hydrometer methods, pycnometers, and gas chromatography[2,3], often have strict temperature requirements, require direct contact with the surface of the object, or use probes, leading to potential contamination and affecting the surface characteristics of the object. With technological advancements, various detection techniques have become increasingly mature. Although technologies like near-infrared (NIR) spectroscopy have been used for liquid component detection, they remain complex and expensive. Therefore, proposing a non-contact measurement method that is simple to operate, highly applicable, and low-cost holds significant importance.

This study aims to provide new ideas and methods for non-contact measurement of liquid components inside containers and to offer scientific evidence for engineering applications and research in related fields. The basic principles and applications of NIR spectroscopy and microwave radar technology will be briefly introduced below.

[1]Department of Mathematica and Information Sciences, Shaoxing University, Shaoxing City, China. [2]Key Laboratory of Artificial Intelligence Applications, Shaoxing University, Shaoxing City, China. [3]Visiting Scholar, Department of AOP Physics, University of Oxford, Oxfordshire, UK. [4]National Engineering Research Center for Chinese CRW (Branch Center), Shaoxing University, Shaoxing City, China. [5]School of Medicine, Shaoxing University, Shaoxing City, China. [6]School of Electronic and Electrical Engineering, University of Leeds, Leeds, UK. [7]Oxford Industrial Holding Group, Hong Kong, China. [8]Weijia Zhang and Xuejing Cao Contributed equally to this work. ✉email: usxmedlab@yeah.net

Wavelength Range	Transmission	Diffuse transmission	Diffuse reflection
Short-wave(750–1100 nm)	Clear liquid	Powdered or granular samples	Physical analysis of sample particle size
Mid-wave(1100–1800 nm)	Dark-colored liquid	Granular samples, turbid liquids	Powdered or granular samples, turbid liquids
Long-wave(1800–2500 nm)	Dark-colored liquid	Turbid liquid	Powdered samples, turbid liquids

Table 1. Near-infrared Spectral Analysis of Samples in Different States[8,9].

Category	Microwaves	Near-infrared
Wavelength	1 mm-1 m	750 nm-2500 nm
Frequency	300 MHz-300 GHz	143THz-428THz
Transparency	Transmission, emission, absorption	Transmission, emission, absorption
Penetrability	Intensity (able to penetrate glass, plastic, ceramics, etc.)	Weak (able to penetrate water, biological tissues under certain conditions)

Table 2. Comparison of Near-Infrared Spectroscopy and Microwave Detection.

Current state of research

Currently, many researchers are using NIR spectroscopy technology to detect liquid components. NIR spectroscopy is based on the vibrational information of hydrogen-containing groups in substances and operates in the wavelength range between visible light and mid-infrared. Since different substances have different absorption spectra, each component in a substance has specific characteristic absorption peaks, making NIR spectroscopy an effective technique for analyzing liquid components.

In 2015, Paiva et al. used ultra-compact NIR spectrophotometers and Fourier-transform NIR spectrometers to detect diesel mixtures adulterated with vegetable oil[4]. In 2016, Liu Fangfang et al. employed NIR spectroscopy to determine changes in digestive tract liquid components based on variations in the characteristic values of digestive wall blood oxygen signals[5]. Wu Yanwei et al. focused on the detection of liquid components and their concentrations, proposing and designing an optoelectronic detection system suitable for on-site detection, which achieved the detection of components and their concentrations in transparent liquids like honey[6]. In 2019, Song Ziwei et al. optimized NIR light sources and designed a liquid detection cell structure based on the characteristics of liquid components and light transmission properties, conducting concentration detection on ethanol–water solution samples[2].

Despite the widespread application of NIR spectroscopy in the field of liquid detection due to its strong penetration and fast processing speed, it is not suitable for the qualitative analysis of complex mixtures and the detection of non-polar flammable liquids[7]. Depending on the state of the sample, different measurement methods must be used to analyze different states of samples with NIR spectroscopy, as shown in Table 1. For instance, when collecting ethanol spectra, the transmission method is effective, especially in the short wavelength range. In contrast, for turbid liquids like emulsions and rice wine, the collection in the mid-wave and long-wave bands is more effective.

Next, near-infrared spectroscopy has shorter wavelengths and cannot penetrate opaque wine containers, making it difficult to detect internal liquor components. Due to the properties of different materials, they can have a significant impact on the emission and propagation of microwaves. Metal materials, with their high conductivity, completely reflect microwaves and allow almost no penetration, which can significantly affect the accuracy of radar measurements. Compared to highly reflective materials such as metal, ceramics and glass have better microwave transmissivity, which ensures the precision and consistency of radar measurements. This helps maintain stable microwave signal transmission during the measurement process and reduces the effects of reflection and attenuation caused by the container materials. As shown in Table 2, compared to near-infrared spectroscopy, microwave wavelengths are longer, offering better penetration capabilities. During measurement, there is no need for direct contact with the sample, effectively overcoming the limitations of traditional measurement methods. When microwaves are emitted towards the sample, they interact with the medium through spatial radiation. Microwave transmission[10]exhibits excellent characteristics, remaining largely unaffected by smoke, dust, flames, temperature variations, or chemical atmospheres during the transmission process[11]. These characteristics provide a more feasible solution for non-contact detection of alcoholic liquid components inside containers.

Verification of the numerical relationship between total acid content and radar scattering capability

Radar Cross Section (RCS) describes the effective scattering area of an object under radar wave interaction, where electromagnetic waves are emitted, reflected back from the object's surface, and received by the antenna. A lower RCS indicates less electromagnetic wave return from the object's surface, whereas a higher RCS signifies stronger scattering capability of the object to radar waves[12]. In radar scattering, liquids with stronger polarity typically undergo polarization within the electromagnetic field, where internal positive and negative charges rearrange under external electric field influence. Hence, liquids with stronger polarity[13] may exhibit higher RCS values in radar scattering.

Specifications of the VTRIG radar			
Transceiver	40 Tx/Rx	Stop-Start Minimum Step	150MHz
Frequencies	62–69 GHz	PCB board size	80×80 mm
Relative bandwidths	10–800 kHz	Plexiglass cover size	90×90 mm
Field of View (FoV)	Refer to Antenna and RF Characteristics	EIRP (Typ.)	−5 dBm

Table 3. Specifications of the VTRIG radar.
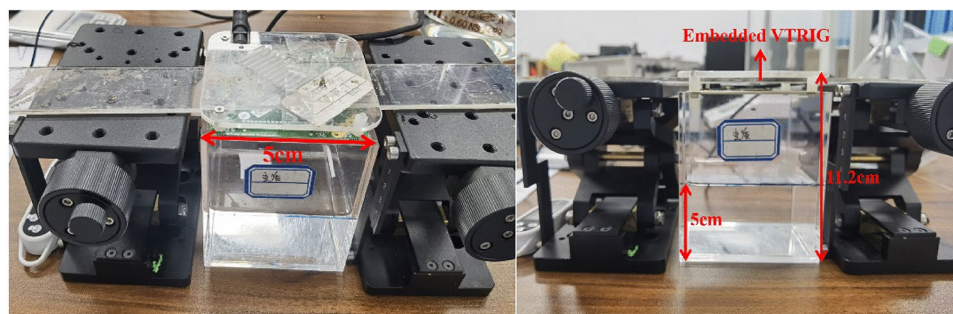
Fig. 1. VTRIG device testing schematic. The heights of the lift platforms on both sides and the liquid level are kept consistent. The left side shows a top-down view, while the right side displays a front view.

According to empirical parameters proposed by Reichardt[14], the polarity level of common solvents partly correlates with changes in RCS[15]. Additionally, RCS varies with angle, frequency, and polarization[16]. Thus, radar detection results can to some extent reflect the polarity characteristics of liquids. However, it's important to note that polarity is a relative concept influenced by factors such as molecular structure, necessitating further consideration in specific experiments and analyses.

Through extensive preliminary experiments with samples, the team observed that severely deteriorated rice wine exhibited stronger polarization reactions than water. This phenomenon may be related to changes in the liquid components of rice wine, such as esterification reactions between lactic acid bacteria and ethanol, leading to the breakdown of less polar ethanol and an increase in the proportion of more polar substances like lactic acid. To verify this observation, the team designed experiments exploring the relationship between total acidity in rice wine[17] and radar scattering capability, further investigating the high-frequency electromagnetic polarization effects of deteriorated rice wine.

Experimental method

Main instruments and reagents

The experiment requires a variety of materials and equipment. These include rice wine from the year 2019, sodium hydroxide standard titration solution, distilled water, custom acrylic containers, a thermometer for temperature measurement, VTRIG radar equipment for measurements (Specific radar parameters can be found in Table 3), an MS-H-Pro+ magnetic stirrer for mixing, a pipette for precise liquid handling, a Z-axis manual lift platform (HTZ-120) for adjusting heights, an acidometer for acidity measurements, and a ruler for dimensional checks. These tools and reagents are essential for conducting accurate and controlled experiments to explore the properties and behaviors of the samples under study.

The VTRIG system integrates a millimeter-wave frontend and an analog baseband signal chain, supporting signal paths for up to 40 antennas. A high-performance synthesizer generates frequency-stepped continuous wave (CW) signals and controls the frequency and scanning of the transmitting antennas. The system accesses the Vayyar API to connect to the VayyarEVK engine, supporting the integration of non-contact radio frequency sensors into user-developed systems. The API is compatible with Python and MATLAB and is suitable for the Windows platform.

Control of experimental conditions

Adjust the heights of the lift platforms on both sides to ensure that the radar is at a consistent height during each test, as shown in Fig. 1. The lift platforms, container, and the sample being measured should always remain in a relatively static position. The experimental samples are placed in a transparent acrylic container ($8cm \times 8cm \times 10cm$) positioned vertically with respect to the tabletop, and the temperature is adjusted to 26℃ (this temperature is based on the measurement taken during the first test at the start of the experiment). The liquid level is consistently maintained at 5cm, and testing is conducted only after the liquid surface is still and free of bubbles to minimize the impact of external factors on the radar cross-section measurement results.

Sample testing

To ensure the accuracy and repeatability of the experiment, total acidity measurement[18] is conducted as follows:

10 mL of sample is pipetted into a 150 mL beaker, followed by the addition of 50 mL of degassed water. As shown in Fig. 2, a magnetic stirring bar is placed in the beaker, which is then positioned on a magnetic stirrer and set into motion. Sodium hydroxide standard titration solution is titrated into the beaker until reaching pH 8.20, with the volume of 0.1 mol/L sodium hydroxide solution consumed recorded. Simultaneously, a blank test with the same volume of degassed water is conducted to record the corresponding volume of titration solution consumed.

Run the code to obtain the imaging values under current conditions (detailed code provided in the Appendix), and perform 10 measurements for each case. During each test, the stability of the device can be ensured by referring to the x-axis data corresponding to the imaging values.

Data processing and analysis
The analysis of rice wine total acidity data utilizes the following mathematical models:

$$X = \frac{(V_1 - V_2) \times C \times M}{V_3} \tag{1}$$

where X represents the total acidity content in the sample, C is the concentration of the sodium hydroxide standard titration solution, M is the molar mass of lactic acid, V_1 is the volume of sodium hydroxide standard titration solution consumed during titration of the test sample, V_2 is the volume consumed during the blank test with sodium hydroxide standard titration solution, and V_3 is the volume of the sample taken for analysis.

The square of radar imaging values Y for different liquids is directly proportional to RCS. Therefore, Y^2 is used as an indicator of radar scattering capability level y:

$$y = Y_{k-r}^2 = \left(\sum_{t=1}^{N_1} \sum_{r=1}^{N_2} \sum_{f} \frac{X_{f,t,r}}{g_{f,k,t,r}} \right)^2 \tag{2}$$

where Y_k is the received value at target position k, $X_{f,t,r}$ is the received frequency domain signal of electromagnetic waves with frequency f, transmitted from antenna t to antenna r corresponding to the channel. $g_{f,k,t,r}$ is the frequency response of the channel corresponding to position k when electromagnetic waves with frequency f are transmitted from antenna t to antenna r. After completing the radar testing of the liquid, calculate the average imaging value of the tested liquid, and generate images for comparison and analysis.

In regression analysis, the goodness of fit R^2 is used to explain the relationship between x and y and the degree of influence[19]:

$$R^2 = \frac{SSR}{SST} = \left(1 - \frac{SSE}{SST} \right) = \left(1 - \frac{\sum_{i=1}^{n} (y_i - \widehat{y}_i)^2}{\sum_{i=1}^{n} (y_i - \overline{y})^2} \right) \tag{3}$$

where SST is the total sum of squares of the original data y_i, SSR is the sum of squares explained by the fitted line, and SSE is the sum of squares of residuals. Detailed data for testing, formula details, and derivations can be found in the Appendix.

Fig. 2. Schematic of the magnetic stirrer. The left side shows the stirrer without a beaker, and the right side shows the stirrer with a beaker and a magnetic stirring bar placed inside. Once the stirrer is turned on, the magnetic stirring bar creates a stirring effect in the liquid.
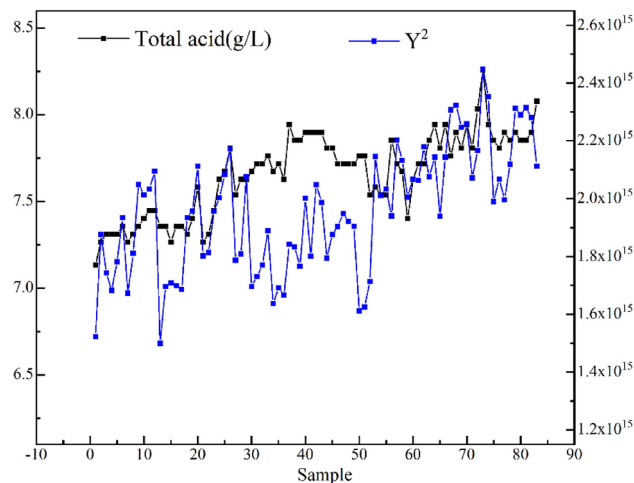
Fig. 3. The horizontal axis represents the first group of 83 samples, with the left vertical axis showing the total acid content of each sample (g/L), corresponding to the black line graph. The right vertical axis corresponds to the blue line graph, whose values are positively correlated with the RCS level. The specific relationship between the RCS level and the original data is recorded in the Appendix.

DV	Source	Square sum	df	Mean square	F	P
	Inter group	210.946	2	105.473	679.122	0.000
x	Within the group	23.296	150	0.155		
	Total	234.242	152			
	Inter group	2.89129	2	1.445^29	3.903	0.022
y	Within the group	5.55530	150	3.703^28		
	Total	5.84430	152			

Table 4. Analysis of Differences in Total Acidity and Imaging Values among Different Groups. Note: p < 0.01 indicates highly significant differences; 0.01 < p < 0.05 indicates significant differences; p > 0.05 indicates no significant differences.

Results analysis

As shown in Fig. 3, during the induction of Rice wine spoilage in the first group of samples, x and y show an overall increasing trend. Statistical analysis of group, total acidity content, and radar scattering levels helps further understand the interaction characteristics between radar waves and samples.

Analysis of differences in total acidity and radar scattering capability across different groups
The test subjects were categorized into three groups based on their composition: the first group consisted of rice wine and yeast, the second group of rice wine and water, and the third group of rice wine and spoiled rice wine. Due to the different compositions of the samples, there may be varying trends in the subsequent changes of x and y. The sample group was treated as the independent variable, and a one-way analysis of variance (ANOVA) was conducted on the measurement data, followed by post-hoc tests for further clarification.

Table 4 shows that there is a highly significant difference in total acidity among the different groups (p < 0.01), and the difference in radar scattering capability among the groups is significant (p < 0.05). The results of the LSD post-hoc test indicate that there is no significant difference (p > 0.05) in radar scattering capability between the second and third groups, as shown in Table 5.

Correlation analysis of total acidity and radar scattering capability among different groups
As shown in Table 6, radar scattering levels are influenced by polar substances such as total acidity. There is a correlation between total acidity and radar scattering capability in each group. In the first group, x and y are highly significantly positively correlated (p < 0.01); in the second group, x and y are also highly significantly positively correlated (p < 0.01); in the third group, x and y are significantly positively correlated (p < 0.05).

The total acid content of different groups is used as the independent variable x, and the radar scattering capability is used as the dependent variable y to conduct regression analysis. The specific analysis results are shown in Table 7.

The model formula for the first group is: $y = -1.808^{15} + 4.914^{14}x$. The R^2 is 0.300, indicating that total acidity can explain 30.0% of the variation[20] in RCS (Radar Cross Section). The model also passed the F-test (F = 34.694, p = 0.000 < 0.05), indicating that changes in total acidity significantly affect radar scattering

DV	Group	Group	Mean difference (I-J)	Standard error	P
x	1	2	−2.243*	0.079	0.000
		3	1.130*	0.079	0.000
	2	1	2.243*	0.079	0.000
		3	3.374*	0.094	0.000
	3	1	−1.130*	0.079	0.000
		2	−3.374*	0.094	0.000
y	1	2	−8.20613*	3.878^13	0.036
		3	−9.19313*	3.878^13	0.019
	2	1	8.20613*	3.878^13	0.036
		3	−9.87112	4.600^13	0.830
	3	1	9.19313*	3.878^13	0.019
		2	9.87112	4.600^13	0.830

Table 5. Post-hoc comparison of the effects on total acidity and imaging values among different groups. Note: * indicates significance, p < 0.05.

Group	Index	x^1	y^1	x^2	y^2	x^3	y^3
1	x^1	1	0.548**	0.745**	0.730**	0.762**	0.379**
	y^1	0.548**	1	0.151	0.030	0.434**	0.622**
2	x^2	0.745**	0.151	1	0.826**	0.690**	−0.106
	y^2	0.730**	0.030	0.826**	1	0.700**	−0.152
3	x^3	0.762**	0.434**	0.690**	0.700**	1	0.194*
	y^3	0.379**	0.622**	−0.106	−0.152	0.194*	1

Table 6. Correlation between total acidity and scattering capability. Note: **. Significant at the 0.01 level (two-tailed); *. Significant at the 0.05 level (two-tailed).

Group	Model	R^2	Beta	F	P
1	$y = -1.808^{15} + 4.914^{14}x$	0.300	0.548	34.694	0.000
2	$y = 2.582^{14} + 1.798^{14}x$	0.682	0.826	70.732	0.000
3	$y = 5.047^{14} + 3.059^{14}x$	0.214	0.462	8.970	0.005

Table 7. Regression Analysis of Total Acid Content on Radar Scattering Capability Among Different Groups. Note: The dependent variable y represents radar scattering capability, while the independent variable x denotes total acid content. F denotes the result of the F-test.

capability. As shown in Fig. 2, the overall trend of total acidity and radar scattering capability for the first group can be observed.

The second group shows a significant change in the F value (F = 70.732, p = 0.000 < 0.05), indicating that total acid content has a significant impact on radar scattering ability, which is statistically significant[21]. In addition, the R^2 has increased to 0.682, suggesting that total acid content can explain 68.2% of the variance in radar scattering ability.

For the third group, the R^2 is 0.214, and the model did not pass the F-test (F = 70.732, p = 0.005), indicating that total acid content does not have a significant impact on radar scattering ability.

From Fig. 4, it can be seen that although the trends in total acid content vary among the groups, they all affect radar scattering levels and show a positive correlation. Therefore, we infer that in radar scattering, the increase in polar substances like total acid leads to higher RCS values in the samples. Additionally, analyzing the data in the Appendix for each group shows that the first group has the highest average total acid content, reaching 9.90 g/L. The second group has the lowest total acid content, but the highest radar scattering level. This might be because, at the same temperature, the polarity of distilled water and acids is greater than that of alcohols, with distilled water having a higher polarity level than acids[22,23].

Future research could explore the relationship between other components in alcoholic beverages and radar scattering characteristics to further enhance the analysis and identification capabilities of samples. It should be noted that the above is only a preliminary analysis and is influenced by multiple factors, including the physical properties of the samples and the complexity of the interaction between radar waves and the samples.
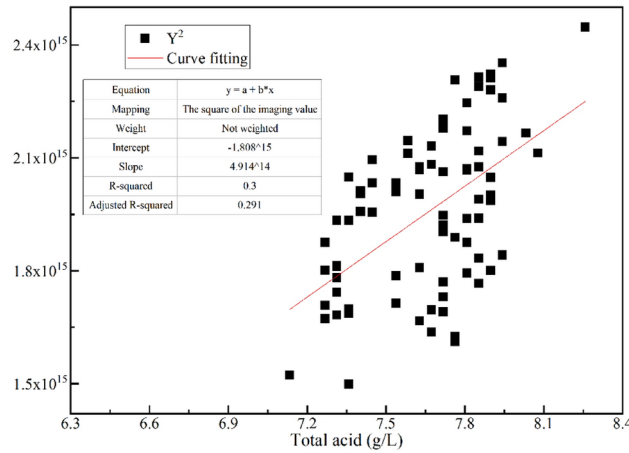
Fig. 4. Scatter plot of total acid content versus radar scattering ability. The horizontal axis represents the total acid content of the corresponding samples (g/L), while the vertical axis, Y^2, represents the radar scattering ability. The overall trend of the data can be visually observed from the distribution of the scatter points. In the upper left corner, the model evaluation parameters obtained from the regression analysis of the data are displayed.

The derivation and validation of the principle of RCS measurement of liquid components
Theoretical derivation

In microwave detection, the electromagnetic characteristics of homogeneous dielectric materials are described by permeability μ, permittivity ε, and conductivity γ. Different components in a mixture have different permittivities, which lead to changes in the microwave signal's characteristic parameter, namely the return loss (Ma[26]). Changes in return loss result in variations in the RCS level of the measured object. Based on electromagnetic scattering theory, the radar scattering ability of a liquid can be converted into changes in the electromagnetic parameters of the measured liquid. When the composition of the mixture changes, the microwave field is affected, converting the composition change into variations in microwave characteristic parameters. By measuring these microwave parameters, the composition of the mixed liquid can be identified.

As a form of electromagnetic wave, microwaves propagate in media according to the laws of electromagnetic wave transmission[24]. Due to the different intrinsic impedances Z of various media, the ratio of the electric field E to the magnetic field H also varies:

$$\frac{E_i}{H_i} = \frac{E_r}{H_r} = Z_1 = \sqrt{\frac{\mu_1}{\varepsilon_1}} \tag{4}$$

$$\frac{E_t}{H_t} = Z_2 = \sqrt{\frac{\mu_2}{\varepsilon_2}} \tag{5}$$

where E_i, E_r and E_t are the electric fields of the incident, reflected, and transmitted waves, respectively, and H_i, H_r and H_t are the magnetic fields of the incident, reflected, and transmitted waves, respectively. μ_1 and ε_1 are the permeability and permittivity of medium 1, and μ_2 and ε_2 are the permeability and permittivity of medium 2. These parameters must also satisfy the boundary conditions at the interface between the media. At the interface between the media:

$$E_i + E_r = E_t \tag{6}$$

$$H_i - H_r = H_t \tag{7}$$

Substitute (4) and (5) into (7) to solve:

$$\frac{E_i}{Z_1} - \frac{E_r}{Z_1} = \frac{E_t}{Z_2} \tag{8}$$

By solving (6) and (8) simultaneously, the reflection coefficient Γ at the interface, when microwaves propagate from medium 1 into medium 2, is:

$$\Gamma = \frac{E_r}{E_i} = \frac{Z_2 - Z_1}{Z_2 + Z_1} = \frac{\sqrt{\frac{\mu_2}{\varepsilon_2}} - \sqrt{\frac{\mu_1}{\varepsilon_1}}}{\sqrt{\frac{\mu_2}{\varepsilon_2}} + \sqrt{\frac{\mu_1}{\varepsilon_1}}} = \frac{\sqrt{\frac{\mu_{r_2}\varepsilon_{r_1}}{\mu_{r_1}\varepsilon_{r_2}}} - 1}{\sqrt{\frac{\mu_{r_2}\varepsilon_{r_1}}{\mu_{r_1}\varepsilon_{r_2}}} + 1} \tag{9}$$

where $\mu_1 = \mu_0\mu_{r1}, \varepsilon_1 = \varepsilon_0\varepsilon_{r1}, \mu_2 = \mu_0\mu_{r2}, \varepsilon_2 = \varepsilon_0\varepsilon_{r2}; \mu_0 = 1.25 \times 10^{-6} H/m, \varepsilon_0 = 8.854 \times 10^{-12} F/m$ are the permeability and permittivity of vacuum. And μ_{r1}, ε_{r1}, μ_{r2}, ε_{r2} are the relative permeability and permittivity of medium 1 and medium 2.

From (9), it can be seen that when the composition of the mixed liquid changes, the permeability μ and the permittivity ε will also change, leading to a corresponding change in the reflection coefficient. The return loss (RL), which refers to the loss in dB between the microwave feedback signal and the incident signal, is related to the reflection coefficient as follows[25]:

$$RL = -10\lg\left(\frac{P_r}{P_t}\right) = -20\lg|\Gamma| \tag{10}$$

$$RL = -10\lg(\frac{P_r}{P_t}) \tag{11}$$

Combining with the radar equation:

$$P_r = \frac{P_t G_t}{4\pi r^2}\sigma\frac{1}{4\pi r^2}A_{eff} \tag{12}$$

where P_t is the radar transmission power, P_r is the received radar power, r is the distance from the radar to the detected target, A_{eff} is the effective area of the receiving antenna, G_t is the radar antenna gain, and σ is the target's RCS. It can be derived that the electromagnetic properties of liquid components relate to σ as follows:

$$\left|\frac{\sqrt{\frac{\mu_{r2}\varepsilon_{r1}}{\mu_{r1}\varepsilon_{r2}}}-1}{\sqrt{\frac{\mu_{r2}\varepsilon_{r1}}{\mu_{r1}\varepsilon_{r2}}}+1}\right|^2 = \frac{P_r}{P_t} = \frac{G_t}{4\pi r^2}\sigma\frac{1}{4\pi r^2}A_{eff} \tag{13}$$

RCS experiment setup

Main instruments and reagents

Vector Network Analyzer SNA5032A ((refer to Table 8 for detailed specifications), standard gain horn antenna (12 GHz ~ 18 GHz), power amplifier (JL-PA08018025-P23), DC power supply, stand, ceramic jars, pipetting device, rice wine (from Cheng Huangjiu Industry), distilled water, ethanol, 5% acetic acid solution, formamide, kerosene.

Control of experimental conditions

The experimental environment is kept constant, with the room temperature controlled at 26 degrees Celsius to avoid interference from other objects in the environment on the radar signals. Additionally, the wine jar is placed horizontally on a wooden table that is perpendicular to the ground, and the position of the jar is marked from the beginning to ensure consistency between the radar irradiation angle and the direction of signal incidence. Before to use, calibrate the vector network analyzer to ensure optimal performance. Adjust the height of the horn antenna so that it is positioned below the wine jar, ensuring proper alignment for the experiment.. To minimize the impact of radar transmission power fluctuations, we utilized a stable power supply and regularly calibrated the radar equipment.

The vector network analyzer increases signal bandwidth at the cost of time by emitting frequency-stepped signals, resulting in one-dimensional high distance resolution for the tests. Its time-domain functionality significantly reduces the requirements for the testing environment, enabling high-precision measurements.

Testing procedure

As shown in Fig. 5, this experiment utilizes an RCS frequency-stepped testing system. It employs a standard gain horn antenna to transmit and receive electromagnetic wave scattering signals. The frequency response received by the vector network analyzer is transformed into time-domain response using inverse fast Fourier transform (IFFT), yielding corresponding measurement values. This validates whether the RCS frequency-stepped testing system can measure the radar cross-section of radar targets inside containers and differentiate between different liquids within the containers.

The process is detailed as follows:

Parameter	Specification
Frequency range	100kHz-13.5GHz
Amplitude resolution	1Hz
Intermediate frequency bandwidth range	0.05dB
Dynamic range	10Hz-3MHz
Maximum output power	10dB

Table 8. Parameters of the vector network analyzer SNA5032A.
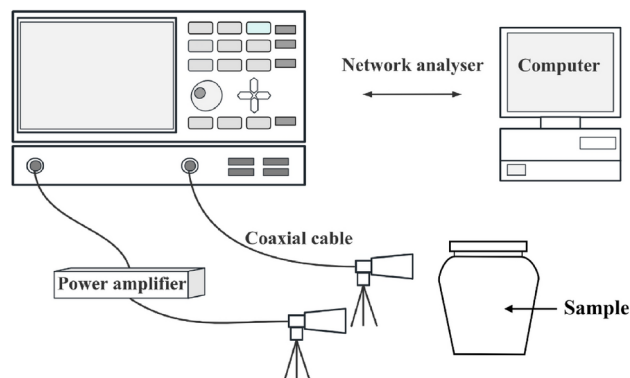
Fig. 5. Dielectric measurement experimental device.

Step 1: Calibrate the vector network analyzer. Adjust the horn antenna height to be below the opening of the container and maintain this height throughout. Connect the output port to the power amplifier and then to the transmitting antenna. Connect the input port to the receiving antenna. Position the test container 50 cm away from the standard gain horn antenna.

Step 2: The vector network analyzer emits frequency-stepped signals and measures the frequency domain response of the empty jar. Utilize the time-domain transformation function of the vector network analyzer to convert the frequency domain response into the time domain. Set the starting time of the time domain to 0 s and store the time-domain response data in the vector network analyzer's register.

Step 3: Introduce the solution into the container, ensuring the liquid level is above the horn antenna height. Store the time-domain response data in the vector network analyzer's register. Use a pipetting device to empty the liquid from the jar, ensuring the container's position remains unchanged.

Finally, repeat the above experimental steps 3–4 times to measure the same liquid, ensuring data accuracy. Once confirmed, introduce another solution and measure its frequency domain response. Convert the frequency domain response into the time domain and store the time-domain response data in the vector network analyzer's register. Repeat this process 3–4 times.

Through these steps, the team obtained time-domain response data for empty jars, jars containing water and rice wine, as well as empty glass beakers, glass beakers containing water, ethanol, 5% acetic acid solution, formamide, and kerosene, for further analysis.

Measured results and analysis

Experimental results

Below are the vector network analyzer test results for ceramic jars in three different states: empty, filled with water, and filled with rice wine. The experimental results for glass beakers are found in the Appendix.

Comparing Fig. 6 and Fig. 7, it is observed that the peak values displayed on the vector network analyzer for the ceramic jar filled with water show a significant difference of approximately 7 dB, while the overall waveform remains unchanged. This indicates that the frequency-stepped testing system is capable of penetrating the ceramic jar. Additionally, the scattering field intensity changes after adding liquid, leading to variations in RCS, which are observable on the vector network analyzer.

Furthermore, multiple measurements of the empty jar and the jar filled with water show nearly identical waveforms at each peak value. Minor differences observed may be attributed to experimental noise and are considered valid data. In contrast to the jar filled with water, the empty jar exhibits another larger peak, suggesting that electromagnetic waves not only pass through the front wall of the jar but also penetrate to the rear wall and undergo continuous reflection inside the jar, resulting in a larger peak. The jar filled with water, however, does not exhibit a second larger peak likely due to the strong absorption of electromagnetic waves by the liquid.

Observations from Fig. 7 and Fig. 8 reveal that the peak values displayed on the vector network analyzer for the ceramic jar filled with water and rice wine show variations of approximately 1 dB, while the overall waveform remains unchanged. This indicates that the jars filled with water and rice wine have different RCS, and these differences are reflected in the measurement values on the vector network analyzer.

Moreover, multiple measurements of the empty jar and the jar filled with water show nearly identical waveforms at each peak value, with any discrepancies likely attributable to experimental noise and thus considered valid data.

Overall, the frequency-stepped testing system effectively distinguishes between different liquids inside ceramic jars. To further distinguish changes in the aging process of rice wine inside the jar, additional analysis of data from different stages of rice wine is necessary.

Numerical calculation

Figure 9 represents a microwave transmission channel with containers and different liquids as media. When propagating from medium 1 to medium 2, according to formula[14], the σ ratio can be calculated for different states.
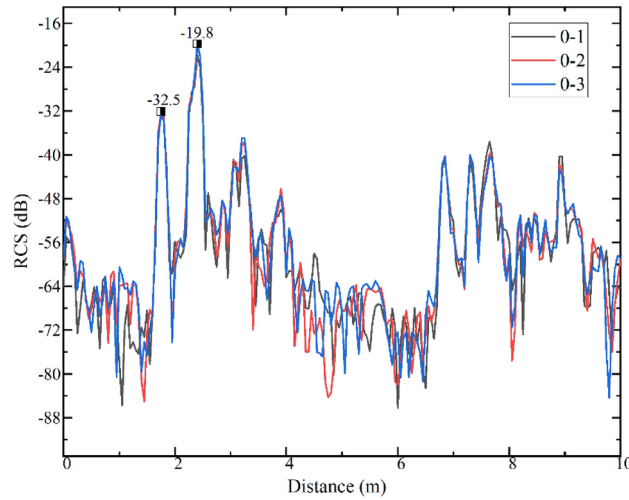
Fig. 6. The vector network analyzer obtained time-domain response measurements for the empty ceramic jar. Three tests were conducted on the same object at different times, represented by gray, blue, and red lines. The horizontal axis shows the distance change converted from the speed of electromagnetic wave propagation, while the vertical axis represents the RCS (dB).
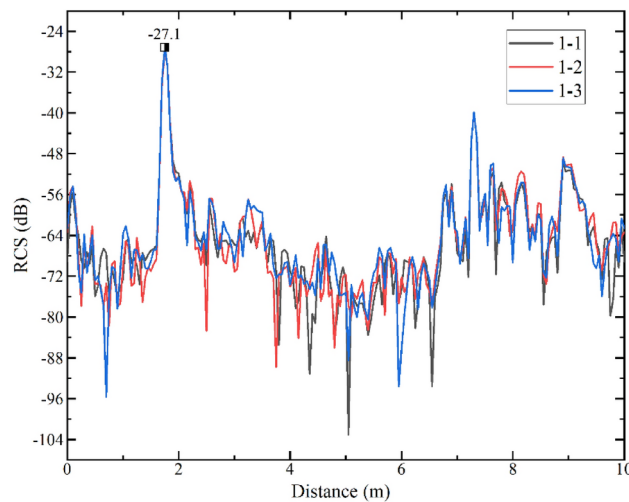
Fig. 7. The vector network analyzer obtained time-domain response measurements for the ceramic jar filled with water. Three tests were conducted on the same object at different times, represented by gray, blue, and red lines. The horizontal axis shows the distance change converted from the speed of electromagnetic wave propagation, while the vertical axis represents the RCS (dB).

The ratio of the measured σ_{dB}^1 before each liquid group to the σ_{dB}^2 measured afterward is denoted as Y_1, while the theoretical ratio is denoted as Y_2:

$$Y_1 = \frac{\sigma^1}{\sigma^2} = 10^{\frac{\sigma_{dB}^1 - \sigma_{dB}^2}{10}} \tag{14}$$

$$Y_2 = \frac{\sigma^1}{\sigma^2} = \left| \frac{\sqrt{\frac{\mu_{r2}^1 \varepsilon_{r1}^1}{\mu_{r1}^1 \varepsilon_{r2}^1}} - 1}{\sqrt{\frac{\mu_{r2}^1 \varepsilon_{r1}^1}{\mu_{r1}^1 \varepsilon_{r2}^1}} + 1} \right|^2 \left| \frac{\sqrt{\frac{\mu_{r2}^2 \varepsilon_{r1}^2}{\mu_{r1}^2 \varepsilon_{r2}^2}} - 1}{\sqrt{\frac{\mu_{r2}^2 \varepsilon_{r1}^2}{\mu_{r1}^2 \varepsilon_{r2}^2}} + 1} \right|^2 \tag{15}$$

Error analysis
Calculate the average measurement values for each group of objects, as shown in Table 9. The order of measurement values by the vector network analyzer is air, ethanol, 5% acetic acid, formamide, and water. Comparing the
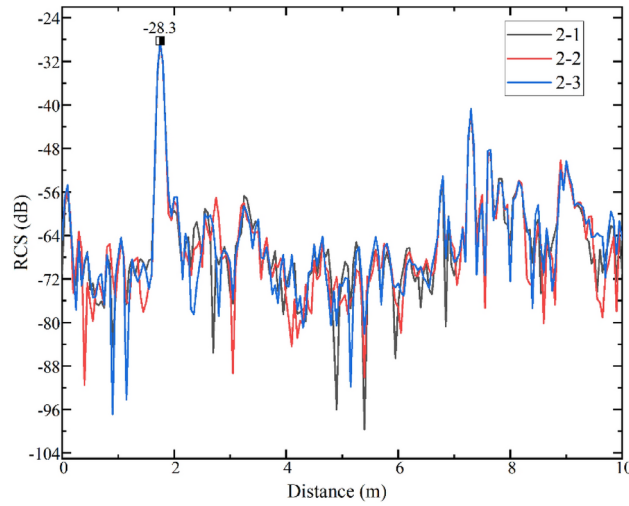
Fig. 8. The vector network analyzer obtained time-domain response measurements for the ceramic jar filled with rice wine. Three tests were conducted on the same object at different times, represented by gray, blue, and red lines. The horizontal axis shows the distance change converted from the speed of electromagnetic wave propagation, while the vertical axis represents the RCS (dB).
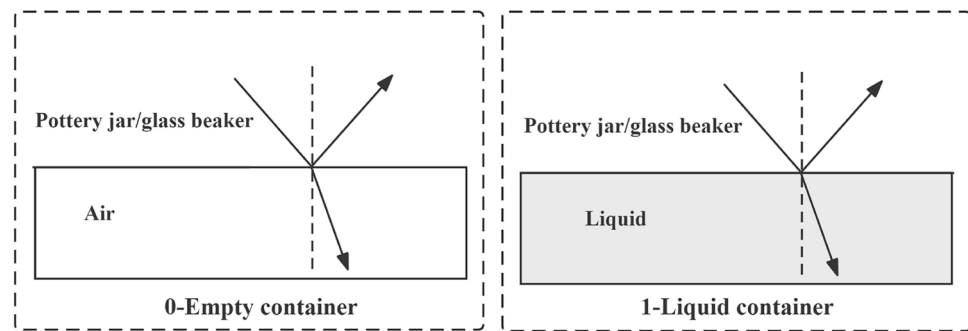
Fig. 9. Simulate the experimental process based on the wave transmission characteristics at the interface of two media for electromagnetic waves.

Categories		X(m)	σ_{dB}^1	σ_{dB}^2	Y_2	Y_1
Ceramic jar	Spoiled rice wine 1	1.7	−33.40	−27.73	-	0.27
	Spoiled rice wine 2	1.75	−39.57	−31.45	-	0.15
	Rice wine 1	1.75	−40.77	−31.72	-	0.12
	Rice wine 2	1.75	−32.56	−28.47	0.36	0.39
	Water 1	1.75	−32.48	−27.47	0.38	0.32
Glass beaker	Ethanol	2.15	−24.02	−26.32	0.19	0.59
	Water	2.15	−24.49	−33.86	0.34	0.12
	Kerosene	2.15	−26.20	−27.57	0.01	0.73
	Formamide	2.15	−24.69	−32.85	0.37	0.15
	5% acetic acid	2.15	−25.49	−31.22	-	0.27

Table 9. The ratio values for different groups.

theoretical and experimental values reveals that the glass beaker group has a larger error, with their order nearly reversed. In contrast, for the ceramic jar group, while there is still some error between theoretical and actual values, they are generally closer.

Possible reasons for this include:

1. Experimental Environment: According to the theoretical definition of radar cross-section (RCS), the distance between the radar and the target must be infinitely large. However, actual experiments are conducted in smaller indoor environments, which can introduce certain testing errors. Compared to ceramic jars, glass beakers have smaller volumes. Electromagnetic waves not only propagate shorter distances in liquids but also scatter less energy overall. Therefore, they are more sensitive to testing distances, which can affect the maximum RCS peak values. Additionally, non-ideal room conditions can introduce noise interference. Background noise includes stray signals entering the receiving antenna from objects other than the target, such as experimental tables, target stands, floors, walls, and other scattered signals (Hu[27]).

2. Testing Position and Angle Errors: This experiment involves near-field RCS. The surfaces of the wine jars are not perfectly consistent, and the rays from each antenna unit to the observation point are not parallel. Changes in the angle and distance of incident waves can lead to variations in the scattering field. Therefore, it is crucial to keep the wine jars and antennas as stationary as possible throughout the experiment. However, changing the liquid inside the wine jars during the experiment can easily alter the jar's position and angle relative to the antenna, resulting in changes in RCS and inaccurate peak data from the vector network analyzer.

3. Container Differences: The preliminary experiments used glass beakers, which have a higher refractive index than typical liquids. At the same time, the ceramic jars used to store rice wine have more pores, leading to structural differences compared to glass beakers. These differences may affect the propagation path of electromagnetic waves to some extent, thereby influencing the measurement values of different groups. In the experiments on the walls, each region presents the same change trend due to the difference in dielectric properties between marble and concrete. Second, the position of region 5 is high, and its extreme value ranks second. The data measured in regions 6 and 9 are very close to the extreme value measured in region 5, and even the extreme value of the data in region 6 exceeds that of region 5. To investigate the reason for this, after dismantling the wall, areas 6 and 9 were not firmly bonded during the filling of the second layer of cement due to operational reasons and gaps. To visualize the experimental results of the wall, a visual image of the extreme data values at 20 cm of the wall is shown in Fig. 11.

Accuracy validation

In the process of alcoholic beverage production, precision testing of each component is crucial to ensuring product quality stability. Many countries and regions have strict regulations regarding the composition of alcoholic products, necessitating accurate testing of alcohol content to ensure compliance. Additionally, in the research and development of alcoholic products, precise testing of component concentrations plays a crucial role. For instance, when developing new alcoholic beverages or adjusting formulations, accurate testing is required to assess the effects of different formulations on product characteristics, thereby ensuring that product quality and taste meet expected standards. Therefore, precision testing of alcoholic beverage components has widespread and significant applications in production, ensuring product quality, regulatory compliance, and consumer health and safety.

Experimental methods

Main instruments and reagents

The materials needed for the experiment include distilled water, ethanol solution, methanol solution, lactic acid solution, funnel, graduated cylinder, glass rod, volumetric flask, plastic pipette, tape, iron stand, and VTRIG radar equipment.

Control of experimental conditions

To ensure the reliability and accuracy of the experiments, the team conducted three months of repeated experiments from May to August 2023. Due to limitations in the accuracy of container calibration and the working time of the testers (the equipment requires one hour of preheating after each startup, and to avoid interference from other factors, solutions of different concentrations were prepared on the same day, making the process time-consuming).

The ambient temperature is maintained at 26 °C. To ensure that the radar's irradiation angle remains consistent relative to the target object, an iron stand is placed on a flat surface, with the fixed angle bracket set at a specific height and marked with a permanent marker. This guarantees that the radar signal's incident direction is always maintained at the designated angle.

Sample testing and data processing

Different concentrations of ethanol solutions were prepared by experimenters. Using 100% ethanol solution as the reference material, appropriate amounts were poured into a volumetric flask based on pre-calculated dilution ratios, diluted with distilled water up to the mark, and then thoroughly mixed. The prepared ethanol solution was slowly poured into a homemade container, as shown in Fig. 10.

After the liquid surface has stabilized, run the code to obtain the imaging values under current conditions. Perform 10 measurements for each case and save the measurement data. Use a siphon to remove the tested liquid, and then clean the container surface with distilled water. After completing the tests on liquids of different concentrations, run the data processing code to calculate the average imaging values of the tested liquids and generate images for comparison and analysis.
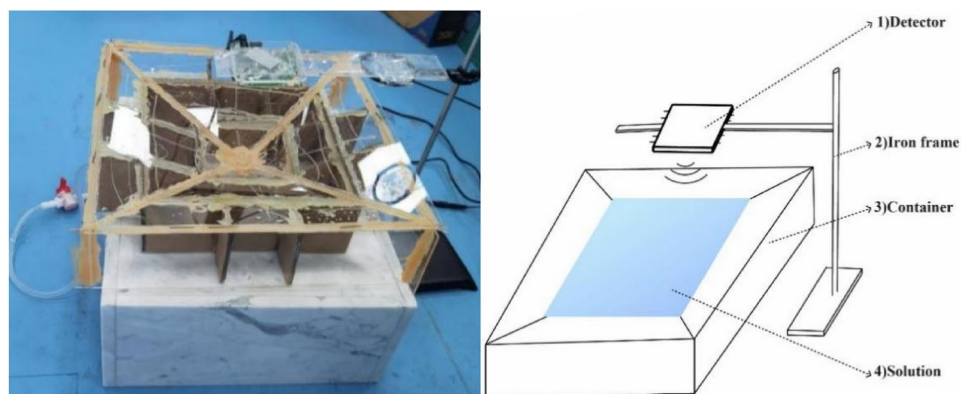
Fig. 10. The setup was specially fabricated by the experimenters, with the radar fixed on top and equipped with a siphon device to clean out the liquid completely after each test. The right figure depicts the initial design sketch before the experiment process.
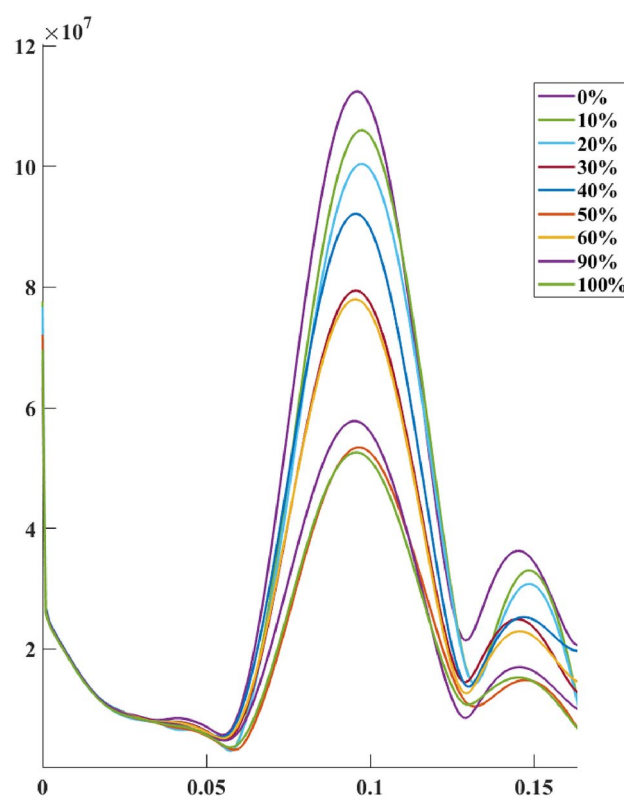
Fig. 11. The radar processed imaging values of ethanol concentrations ranging from 0 to 60%, 90%, and 100% (with 10% intervals) as vertical targets, plotted against the distance from the liquid surface to the radar, measured in meters.

Results and analysis

Experimental results

The experimenters designed and tested solutions of ethanol, methanol, and other substances with gradients ranging from 2 to 10% in concentration. Due to space constraints, we will discuss some selected test scenarios here.

We conducted experiments on a large number of samples, each group arranged in this sequence, with the curve values above representing averaged results. The radar signal detected by the equipment, processed through 'test_shazi.m', showed significant differences. As seen in Figs. 11 and 12, both sets of images exhibit the same pattern: as the concentration of ethanol decreases (the proportion of water increases), the radar scattering capability shows a step-like upward trend. This indicates that our equipment can detect and distinguish solutions with a concentration difference of 2% ethanol or other similar substances. Additionally, multiple experiments
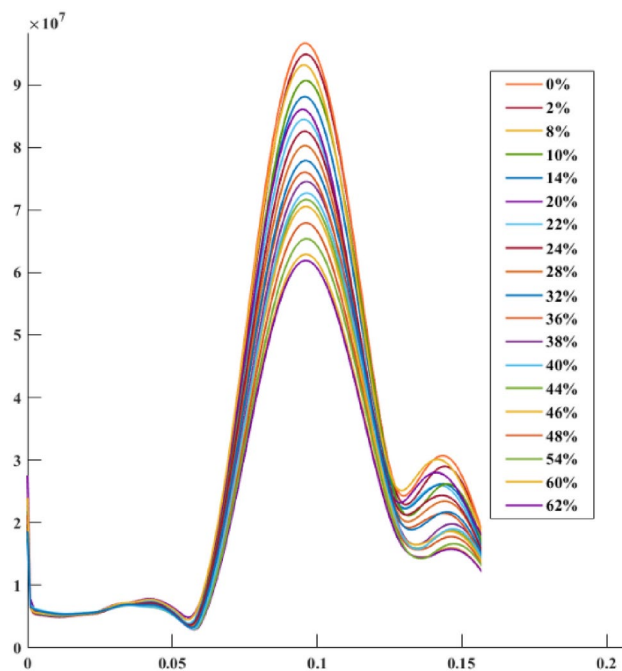
Fig. 12. Vertical axis represents the processed imaging values of ethanol concentrations ranging from 0 to 100% (in intervals of 2%), with distance from the liquid surface to the radar plotted on the horizontal axis, measured in meters.
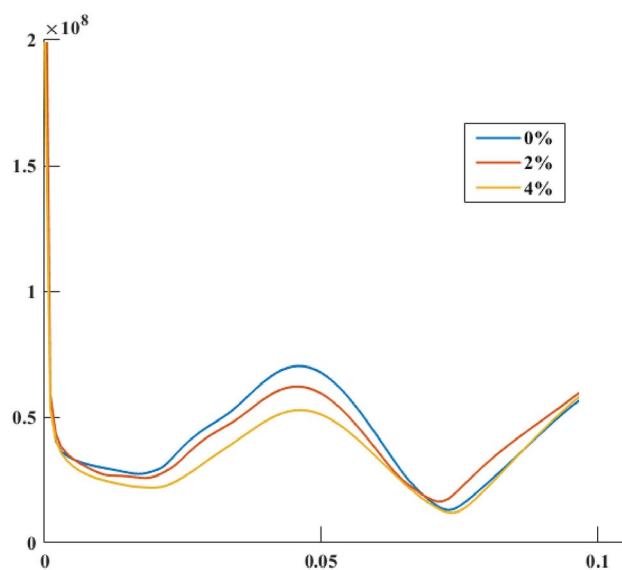
Fig. 13. The vertical axis represents the processed imaging values of lactic acid concentrations ranging from 0 to 4%, with the distance from the liquid surface to the radar plotted on the horizontal axis, measured in meters.

were repeated with solutions of different concentrations spaced at intervals of 2%, 5%, 10%, and 20%, all showing consistent radar imaging results. Figures 13 and 14 show the results for some other types of solutions. This experiment demonstrates excellent repeatability, allowing researchers with suitable facilities to reproduce our findings.

Analysis of the differential radar scattering capability across various concentration levels
Through experiments on solutions such as ethanol, lactic acid, and methanol, it was found that solution concentration affects radar scattering capability. To explore concentration differences among different solutions, this experiment selected three sets of lactic acid data with concentration intervals of 2%, providing a theoretical basis for precision research.
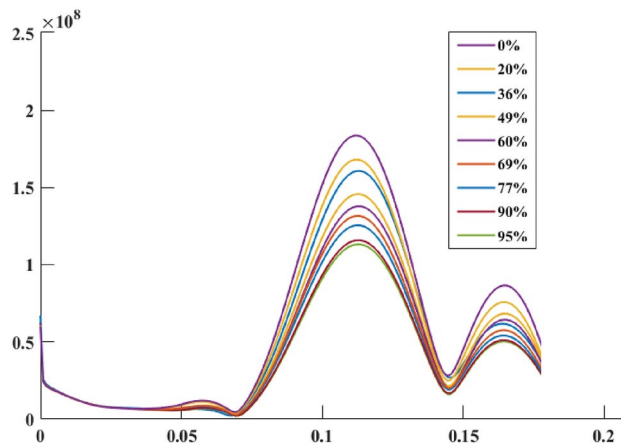
Fig. 14. Imaging values of radar data processed for longitudinal targets with methanol concentration ranging from 0 to 100%, plotted against the distance from the liquid surface to the radar in meters.
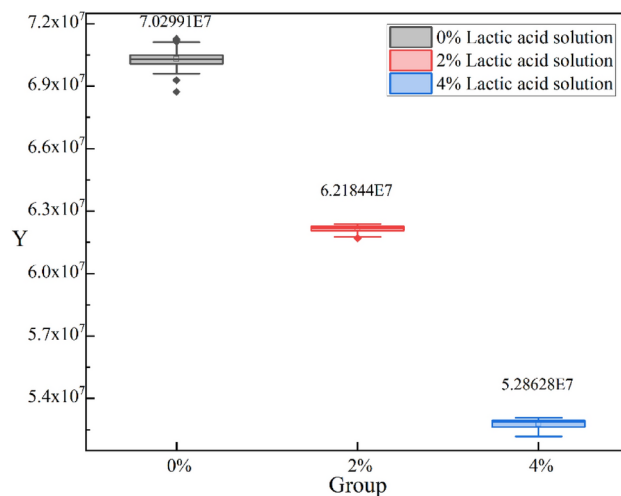
Fig. 15. Box-plot of three concentrations of lactic acid solution.

Source	Square sum	df	Mean square	F	P
Inter group	9.24615	2	4.62315	41,706.859	0.000
Within the group	1.96213	177	1.10911		
Total	9.26615	179			

Table 10. Testing for differences in imaging values of lactic acid solutions at different concentrations. Note: $p < 0.01$ indicates extremely significant; $0.01 < p < 0.05$ indicates significant; $p > 0.05$ indicates not significant.

The box-plot is a statistical graph that describes the distribution of data. As shown in Fig. 15, the value of the line above each box represents the maximum, and the line below represents the minimum. The three lines within the box itself, from top to bottom, represent the values of the 3rd quartile, median, and 1st quartile, respectively. Focusing on different concentrations of lactic acid solutions-0%, 2%, and 4%-a total of 180 sample data sets were analyzed. It is evident that the median values of the three box plots are 7.037, 6.227, and 5.297 respectively. This indicates that in the box plots depicting imaging values from radar equipment for the three liquids, each data set is concentrated, and there are significant differences among the groups.

The data were subjected to one-way analysis of variance (ANOVA). According to Table 10, there are highly significant differences ($p < 0.01$) in the imaging values of lactic acid solutions between different groups.

Improvement strategies

Firstly, before testing, optimization of the sample preparation process is crucial for accuracy in detection. Improving the precision of sample preparation, thorough mixing, and other methods can further enhance detection accuracy, providing more precise data support for subsequent code improvements.

Secondly, during testing, increasing the number of replicate measurements can reduce measurement errors and improve the accuracy of the mean value. Simultaneously, efforts to minimize the influence of interference factors, such as variations in environmental conditions and impurities in samples, ensure experimental stability and enhance detection accuracy.

During the data analysis phase, optimizing data processing methods involves applying more suitable techniques for data handling and analysis to reduce errors and improve precision. This may include employing appropriate statistical analysis methods, machine learning techniques, etc., tailored to the characteristics of the samples and data.

Implementing these measures can significantly improve the accuracy and reliability of alcohol detection. Our team will continue to refine the experimental process based on these aspects to enhance current detection accuracy.

Conclusions

Through microwave radar detection technology, non-contact measurements of internal liquid components in containers were conducted, achieving certain research results. The main conclusions of this study are as follows:

(1) Given the complexity and limitations of near-infrared spectroscopy (NIRS) in liquid component detection, this study introduces microwave detection methods to achieve non-contact detection of liquid components using RCS technology. Microwave detection technology demonstrates unique advantages in analyzing the polar characteristics of liquids.

(2) Through experimental verification, a significant correlation was found between the total acid content and other polar substances with radar scattering capability. The experimental results show that microwave radar can effectively reflect the polar characteristics of liquids, providing a reliable technical foundation for the quantitative analysis of liquid components.

(3) The theoretical analysis indicates that different component liquids exhibit varying electromagnetic properties, which can lead to variations in echo loss and thereby affect RCS levels. Experimental examination of the electromagnetic properties of liquid components reveals the potential of microwave technology in liquid component detection.

(4) The experimental results show that the microwave radar measurement technology used in this study achieved an accuracy level of 2%, effectively distinguishing between different concentrations of ethanol, lactic acid, and other solutions. This further validates the reliability of RCS measurement technology in practical applications.

In conclusion, this study successfully applied microwave RCS measurement technology to the non-contact detection of liquid components. This method demonstrates clear advantages in detecting complex liquids and in non-contact measurement environments, achieving some progress in both experimental accuracy and practical applications, although it cannot completely replace NIR spectroscopy. In the future, as the technology continues to improve and its application scope expands, microwave RCS measurement technology is expected to play a vital role in more fields, providing new ideas and methods for the precise detection of liquid components.

Data availability

All data generated or analysed during this study are included in this supplementary information files.

References

1. Sperber W H. Introduction to the microbiological spoilage of foods and beverages[J]. Compendium of the microbiological spoilage of foods and beverages, 2009: 1–40.
2. Song Ziwei. Research on Multi-band Near-infrared Liquid Component Detection Methods [D]. Heilongjiang University, 2019 (in Chinese).
3. Jespersen, N. Evaluation of basic physical properties[J]. *Compr. Anal. Chem.* **47**, 41–62 (2006).
4. Paiva, M. E. et al. Quantification of biodiesel and adulteration with vegetable oils in diesel/biodiesel blends using portable near-infrared spectrometer[J]. *Fuel* **160**, 57–63 (2015).
5. Liu Fangfang. The Signal-processing and Analytics Methodology of IR Spectrum for Detection of Liquid Components in Stomach [D]. Chongqing University of Posts and Telecommunications, 2016 (in Chinese).
6. Wu Yanwei. A design and its applications of liquid concentration measurement system based on spectrum analysis [D]. Nanjing University of Aeronautics and Astronautics,2017 (in Chinese).
7. Xueshi, Z. et al. Nondestruetive Spectroscopic Methodologies of Flammable Liquids: A Review [J]. *Advances in Laser and Optoelectronics* **58**(02), 23–36 (2021).
8. Jiang Qiaoyong. Model Optimization for Sugar of Rice Wine Based on Near Infrared Spectroscopy [D]. China Jiliang University,2015 (in Chinese).
9. Chernyshova A. Near-infrared (NIR) spectroscopy for food quality applications[D]. Purdue University, 2009.
10. Nicolson, A. M. Broad-band microwave transmission characteristics from a single measurement of the transient response[J]. *IEEE Transactions on Instrumentation and Measurement* **17**(4), 395–402 (1968).
11. Zhang Xintong. Research on Methods and Devices for Moisture Content Detection Based on Microwave Transmission Technology [D]. Jilin University,2015(in Chinese).
12. Chen Na. Research on New Passive Tags in RFID and Sensing Systems [D]. Southeast University, 2020(in Chinese).
13. Yixin, J. et al. Measurement of Liquid Polarity Based on Terahertz Spectroscopy [J]. *Optical Instruments* **41**(03), 1–6 (2019).

14. Reichardt, C. Empirical parameters of the polarity of solvents[J]. *Angewandte Chemie International Edition in English* **4**(1), 29–40 (1965).
15. Zhang, W. et al. Discovery of electromagnetic polarization in Asian rice wine deterioration process and its applications. *PLOS ONE* **19**(6), e0302983 (2024).
16. Merrill I. Skolnik. Introduction to Radar Systems (Third Edition) [M]. Electronics Industry Press, 2014: Chapter 2, page 49.
17. Ni H F, Zhang J P, Huang J P, et al. Rapid determination of total acid content in pre-fermentation process of rice wine by near infrared spectroscopy[J]. 2020.
18. GB/T13662–2018. Rice wine[S].
19. Barassi, R. M. Microeconometrics; Methods and Applications [J]. *The Economic Journal* **116**(509), F161–F162 (2006).
20. Zhou Jun, Ma Shipeng. SPSSAU Research Data Analysis Methods and Applications. 1st Edition [M]. Electronics Industry Press, 2024 (in Chinese).
21. Dao-de, S. Selection of the linear regression model according to the parameter estimation[J]. *Wuhan University Journal of Natural Sciences* **5**(4), 400–405 (2000).
22. Hemin, X., Yao, Ma. & Zihua, D. Detection of Miscible Liquids Components Based on Microwave Technology [J]. *Modern Chemical Industry* **32**(11), 111–114 (2012).
23. Routray, W. & Orsat, V. Dielectric properties of concentration-dependent ethanol+ acids solutions at different temperatures. *Journal of Chemical & Engineering Data.* **58**(6), 1650–1661 (2013).
24. Song Zhiming, Wang Li, Gao Xiaorong, et al. Reflection and Transmission Characteristics of Electromagnetic Waves at Media Interfaces [J]. Information Technology, 2010, 34(06): 172–175+178 (in Chinese).
25. Bird, T. S. Definition and misuse of return loss [report of the transactions editor-in-chief] [J]. *IEEE Antennas and Propagation Magazine* **51**(2), 166–167 (2009).
26. Ma Yao. Research on Microwave Detection Technology for Mixed Liquid Components [D]. Taiyuan University of Technology, 2013 (in Chinese).
27. Hu Chufeng. Research on Radar Target RCS Testing System and Microwave Imaging Diagnostic Technology [D]. Northwestern Polytechnical University, 2007 (in Chinese).

Acknowledgements

Author contributions

Conceptualization: Weijia Zhang. Data curation:Tianfang Wei, Xuejing Cao. Formal analysis: Tianfang Wei, Xue Cheng. Investigation: Zhaowei Wang, Dongqin Sun. Resources: Calvin Choi,Shaomin Cai, Nutapong Somjit. Supervision: Weijia Zhang, Nutapong Somjit. Validation: Xue Cheng, Tianfang Wei. Writing – original draft: Xuejing Cao,Xue Cheng. Writing – review & editing: Weijia Zhang, Nutapong Somjit.

Funding

Declarations

Competing interests

The authors declare no competing interests.

Additional information

Supplementary Information The online version contains supplementary material available at https://doi.org/10.1038/s41598-024-81043-4.

Correspondence and requests for materials should be addressed to S.C.

Reprints and permissions information is available at www.nature.com/reprints.

Publisher's note Springer Nature remains neutral with regard to jurisdictional claims in published maps and institutional affiliations.